Article

Developmental Cell

A WntD-Dependent Integral Feedback Loop Attenuates Variability in *Drosophila* Toll Signaling

Graphical Abstract

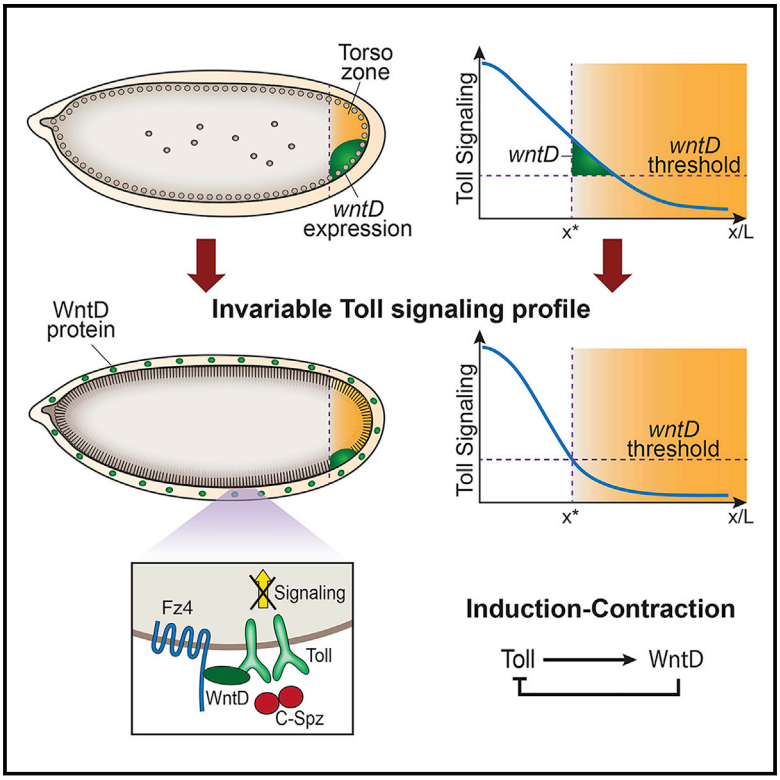

Highlights

- Toll/Torso signaling induces *wntD* embryo expression in a restricted posterior zone
- WntD protein is secreted and uniformly distributed in the extracellular milieu
- WntD binds Fz4 and blocks the Toll extracellular domain, attenuating Toll signaling
- WntD self-inhibits, generating an invariable Toll signaling profile at steady state

Authors

Neta Rahimi, Inna Averbukh, Michal Haskel-Ittah, Neta Degani, Eyal D. Schejter, Naama Barkai, Ben-Zion Shilo

Correspondence

naama.barkai@weizmann.ac.il (N.B.), benny.shilo@weizmann.ac.il (B.-Z.S.)

In Brief

Specification of cell fates along the dorsoventral axis of the *Drosophila* embryo is directed by the Toll signaling pathway. Rahimi et al. show that while embryos initially display considerable variation in Toll pathway signaling magnitude, induction of the expression of an inhibitor, WntD, leads eventually to an invariable pattern.

Rahimi et al., 2016, Developmental Cell *36*, 401–414
February 22, 2016
http://dx.doi.org/10.1016/j.devcel.2016.01.023

Developmental Cell
Article

A WntD-Dependent Integral Feedback Loop Attenuates Variability in *Drosophila* Toll Signaling

Neta Rahimi,[1,2] Inna Averbukh,[1,2] Michal Haskel-Ittah,[1,2] Neta Degani,[1,2] Eyal D. Schejter,[1] Naama Barkai,[1,*] and Ben-Zion Shilo[1,*]
[1]Department of Molecular Genetics, Weizmann Institute of Science, Rehovot 76100, Israel
[2]Co-first author
*Correspondence: naama.barkai@weizmann.ac.il (N.B.), benny.shilo@weizmann.ac.il (B.-Z.S.)
http://dx.doi.org/10.1016/j.devcel.2016.01.023

SUMMARY

Patterning by morphogen gradients relies on the capacity to generate reproducible distribution profiles. Morphogen spread depends on kinetic parameters, including diffusion and degradation rates, which vary between embryos, raising the question of how variability is controlled. We examined this in the context of Toll-dependent dorsoventral (DV) patterning of the *Drosophila* embryo. We find that low embryo-to-embryo variability in DV patterning relies on *wntD*, a Toll-target gene expressed initially at the posterior pole. WntD protein is secreted and disperses in the extracellular milieu, associates with its receptor Frizzled4, and inhibits the Toll pathway by blocking the Toll extracellular domain. Mathematical modeling predicts that WntD accumulates until the Toll gradient narrows to its desired spread, and we support this feedback experimentally. This circuit exemplifies a broadly applicable induction-contraction mechanism, which reduces patterning variability through a restricted morphogen-dependent expression of a secreted diffusible inhibitor.

INTRODUCTION

Developing organisms establish spatial patterns of gene expression and cell fates using inductive molecular cues. These patterns are precise and reproducible, raising the issue of how fidelity is ensured, considering the multitude of signaling events involved. For many of these processes, underlying variability in the expression of critical pathway components, or the size of the embryo or organ, are inevitable. This variability is normally masked by the action of mostly unknown biological mechanisms, which channel (“canalize” [Waddington, 1959]) signaling to a consistent and reproducible output. The capacity to produce an invariant output in the face of stochastic or genetic variation is termed robustness.

Buffering variability is particularly challenging in the case of morphogen gradients, which represent a widely used strategy for patterning cell fields. Morphogens are produced at a restricted source, and spread to neighboring cells to elicit a signaling response. The receiving cells sense not only the presence but also the level of the morphogen they encounter. A single morphogen can elicit several distinct cell fates in a concentration-dependent manner. Spatial variability in the morphogen-distribution profile impinges directly on the allocation of cell fates. Generating a reproducible morphogen-signaling profile is therefore critical for reliable patterning (reviewed in Rogers and Schier, 2011).

A combination of experimental and computational approaches has been exploited to study the basis of robust patterning by morphogens. In fact, the capacity for robust patterning has been used as a criterion for favoring one signaling mechanism over others. Ourselves and others have shown, for example, that the architecture of the signaling cascade provides the basis for buffering variability in the levels of the core signaling pathway components (reviewed in Barkai and Shilo, 2009). However, even if the gradient becomes robust to protein expression levels, morphogen spread still depends on parameters defining its length scale, including diffusion and degradation rates, which are harder to correct for. If these rates change, the scale of the gradient will vary and its spread will need to be readjusted.

Variation in the size of embryos or tissues similarly necessitates an adjustment of morphogen spread. Such adjustment (scaling) requires “measuring” tissue size, and correcting the distribution profile accordingly. While the molecular mechanism providing scaling may differ between pathways, a common emerging theme is that effective measurement of tissue size requires an extracellular feedback protein that is expressed at the “edge” of the field and diffuses rapidly, to impinge on the entire morphogen profile (Ben-Zvi et al., 2011; Hamaratoglu et al., 2011). We reasoned that such localized feedback could buffer not only variations in size, but would apply more broadly to instances where morphogen levels or distribution vary between individuals. Here we explore this possibility, focusing on patterning the *Drosophila* embryonic dorsoventral (DV) axis.

In *Drosophila*, embryonic DV patterning is initiated during oogenesis, where the ventral follicle cells of the egg chamber generate an extracellular matrix that facilitates proteolysis (Sen et al., 1998) (scheme in Figure 1A). During early embryogenesis, this initial cue serves as the basis for DV patterning via the Toll pathway (reviewed in Moussian and Roth, 2005; Stein and Stevens, 2014). A cascade of extracellular proteases culminates in ventrally restricted activation of the protease Easter (Ea) that cleaves the ligand Spätzle (Spz) (Cho et al., 2012). Graded activation of the Toll receptor by Spz, whose peak defines the ventral-most aspect, leads to a corresponding nuclear localization gradient of the transcription factor Dorsal (Dl) within the

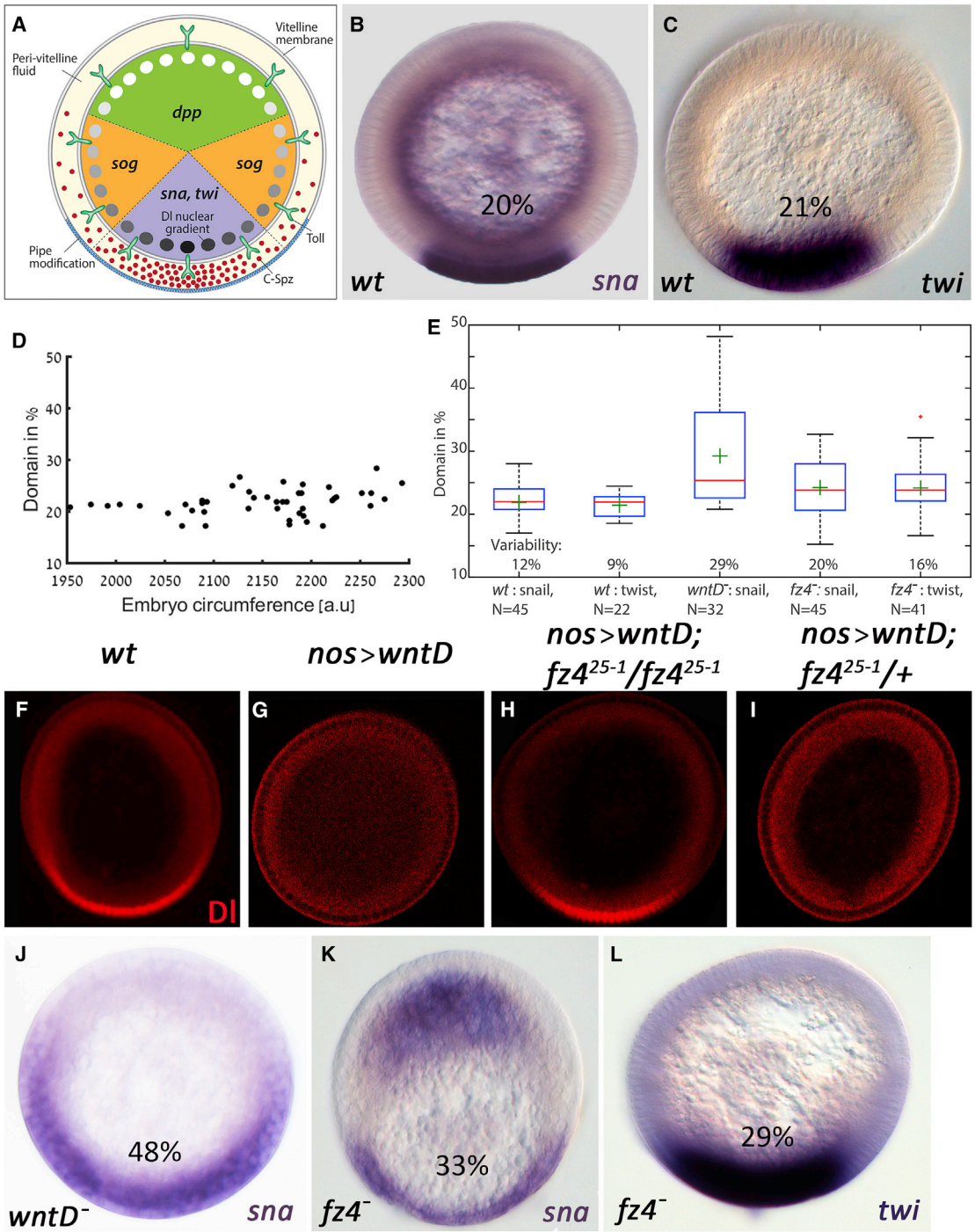

Figure 1. WntD/Fz4 Buffer Variability in Toll Signaling

(A) Early stages of DV patterning. Modification of the ventral vitelline membrane by Pipe during oogenesis generates a permissive surface for processing of Spz during the early stages of embryogenesis. Shuttling of the active moiety C-Spz generates a graded distribution of the ligand with a ventral peak, and following binding to Toll, leads to a corresponding graded nuclear localization of Dl. According to its nuclear levels, Dl defines three distinct domains of zygotic gene expression. The threshold for induction of *sna* expression corresponds to 50% maximal Dl nuclear localization.

(B) Cross section of a *wt* embryo stained for *sna* mRNA.

(C) Cross section of a *wt* embryo stained for *twi* mRNA.

(D) Fraction of the *sna* expression domain from the circumference in a population of *wt* embryos shows low variability, regardless of differences in embryo size.

(E) Variability of the relative size of the *sna* and *twi* expression domains in *wt*, *wntD*, and *fz4* mutant backgrounds. The boxed area defines the 25th–75th percentile of the embryos, and the whiskers extend to the most extreme data points not considered outliers. Mean is in red, and median in green. Variability is calculated as SD divided by the mean.

(legend continued on next page)

embryo (Roth et al., 1989; Rushlow et al., 1989; Steward, 1989). The DI gradient sets the expression pattern of zygotic DV patterning genes, and defines distinct domains along the embryonic DV axis (Figure 1A) (Liberman et al., 2009).

Using a combination of computational and experimental approaches, we recently described the mechanism by which the initial coarse definition of the ventral embryonic domain, where the Spz ligand is processed, leads to sharp activation gradient of the Toll pathway. We described a "self-organized shuttling" mechanism that concentrates the active Spz ligand at the ventral side, relying on diverse interactions between the pro-domain of the ligand and the active moiety (Haskel-Ittah et al., 2012; Shilo et al., 2013). This mechanism is robust to many parameters, but still depends on some key kinetic constants defining its spread. Variability in these parameters could generate embryo-to-embryo differences in the Toll-activation gradient.

Here, we examine the precision of the graded activation of the Toll pathway between embryos, and report that its low variability relies on a buffering mechanism employing the zygotic, posteriorly localized expression of the WntD protein. WntD is secreted and disperses in the extracellular milieu, associates with its receptor Frizzled4 (Fz4), and inhibits the Toll pathway by blocking the extracellular domain of Toll. The levels of *wntD* expression in each embryo depend on the initial Toll signaling levels, providing a negative feedback. Using mathematical modeling, we describe the mechanism by which WntD buffers variability, and show that it exemplifies a broadly applicable buffering mechanism that implements an integral feedback controller. We term this buffering circuit Induction-Contraction (InC).

RESULTS

Low Variability of Toll Signaling

For assessment of the variability of Toll signaling within a population of embryos, it is important to find a reliable benchmark for comparison. Since Toll signaling levels increase during the early phases of embryogenesis (Kanodia et al., 2009; Liberman et al., 2009), a fixed time point is necessary for measurement. Expression of *snail* (*sna*), a zygotic target induced by high levels of nuclear DI, provides such a reliable parameter. *sna* expression is first detected at the beginning of nuclear cycle 14 (Lagha et al., 2013) and displays sharp borders, where the threshold for induction corresponds to ~50% of maximal DI nuclear localization at the ventral midline (Kanodia et al., 2009; Liberman et al., 2009). Once induced the domain of *sna* expression is fixed, maintaining the boundaries of its initial induction. Measurement of the *sna* domain thus provides an approximation of the shape of the Toll-activation gradient at the onset of cycle 14.

For accurate quantitation, cross sections from the center of cycle-14 embryos were monitored for *sna* mRNA by in situ hybridization, and used to calculate the relative fraction of the *sna* domain with respect to the entire circumference of the embryo (Figure S1). We find that the *sna* domain occupies ~21% of the embryo circumference, showing little variability between embryos (12%) (Figures 1B and 1D). During this analysis we observed considerable variability in embryo size, which can be attributed to natural size variability, as well as to the effects of dehydration during fixation. The relative fraction of the *sna* domain from the circumference remains constant, however, and scales with embryo size. In subsequent analyses we will thus present the fraction of the *sna* domain for all embryos in a collection, without allocation to different sizes. Staining for a second DI-induced mesodermal marker, *twist* (*twi*), also showed a low variability between embryos in the relative size of its expression domain (Figures 1C and 1E).

WntD Attenuates Variability in Toll Signaling

The low variability in *sna* and *twi* profiles may indicate a highly reproducible function of the core mechanisms generating the Toll gradient, or alternatively could imply that an additional buffering mechanism impinges on this gradient to reduce its natural variability. Such potential variability can only be uncovered after the buffering mechanism is removed. We speculated that a buffering mechanism could involve an early zygotic transcript encoding a protein that modulates Toll signaling, by either inhibiting or elevating its activity. The secreted WntD protein serves as a potential candidate for this regulatory role, as it is first expressed as an early zygotic gene, and when ectopically overexpressed leads to complete shutoff of Toll signaling (Ganguly et al., 2005; Gordon et al., 2005).

To assess whether WntD normally participates in modulation of Toll signaling, we examined *sna* expression in $wntD^{KO1}$ null embryos (Gordon et al., 2005). This background uncovered a dramatic elevation in variability between embryos (29% in $wntD^{KO1}$ embryos, compared with 12% in wild-type [*wt*] embryos). A significant portion of mutants displayed enlarged *sna* domains of up to 48% of embryo circumference (Figures 1E and 1J). This result clearly demonstrates considerable stochastic effects of the core patterning mechanism, and underscores the normal role of WntD in buffering variability by reducing high levels of Toll pathway signaling.

WntD is a member of the Wnt protein family of secreted ligands that commonly mediate cell-cell signaling by binding to Frizzled multi-pass transmembrane receptors on the receiving cells (Willert and Nusse, 2012). WntD is readily secreted, and lacks the regulatory post-translational modifications typical of other Wnt

(F) DI nuclear localization in a cross section of a *wt* embryo shows a sharp ventrally-biased gradient.
(G) Ubiquitous expression of *wntD* in *nos-Gal4/UAS-wntD* embryos leads to complete dorsalization, as reflected by the exclusion of DI from all nuclei.
(H) Similar expression of *wntD* in $fz4^{25\text{-}1}$ null embryos does not perturb the normal distribution of DI, indicating that Fz4 serves as the receptor for WntD and is essential for its activity.
(I) WntD retains its activity in zygotic $fz4^{25\text{-}1}$ mutant embryos derived from heterozygous $fz4^{25\text{-}1}$ females, indicating that the maternally contributed *fz4* transcripts are in excess.
(J) A $wntD^{KO1}$ mutant embryo displaying an extended *sna* expression domain of 48%.
(K) A $fz4^{25\text{-}1}$ mutant embryo displaying a *sna* domain of 33%.
(L) A $fz4^{25\text{-}1}$ mutant embryo displaying a *twi* domain of 29%. Note: The higher variability in *wntD* mutants compared with *fz4* mutants may be due to backcrossing of the *wntD* mutant to remove second-site modifiers.
See also Figure S1.

proteins (Ching et al., 2008; Herr and Basler, 2012). The Fz4 receptor was previously implicated in WntD activity (McElwain et al., 2011). To examine the involvement of Fz4 in WntD action, we carried out an epistasis analysis. Ectopic expression of *wntD* leads to a complete shutoff of Toll signaling, as reflected by the loss of Dl nuclear localization throughout the entire circumference of the embryo ((Ganguly et al., 2005; Gordon et al., 2005) and Figures 1F and 1G). When combining WntD overexpression with the $fz4^{25\text{-}1}$ null mutant background devoid of both maternal and zygotic contributions, the distribution of Dl was similar to that of *wt* (Figure 1H), demonstrating that Fz4 is obligatory for the inhibitory effect of WntD, and consistent with the notion that Fz4 serves as a receptor for the WntD ligand. *fz4* is expressed maternally and appears to be in excess, since the activity of ectopic WntD was retained in zygotic mutant $fz4^{25\text{-}1}$ embryos derived from heterozygous $fz4^{25\text{-}1}$ females (Figure 1I).

We tested whether *fz4* mutant embryos also display an increased variability in Toll signaling. Indeed, the *sna* expression domain displayed a dramatic increase in variability in this mutant background (Figures 1E and 1K), albeit lower than the one observed in *wntD* mutants. Variability of the *twi* expression domain is similarly affected in *fz4* mutant embryos (Figures 1E and 1L). These observations imply that signaling variability is a fundamental feature of the Toll pathway when it defines the DV axis, and identify WntD/Fz4 as key components of a molecular mechanism employed for buffering this variability.

The Intersection between WntD and Toll Signaling

Since WntD and Fz4 are not considered to be elements of the canonical Toll pathway and are thus likely to function as an auxiliary knob, we wanted to determine where the two pathways intersect. Ectopic WntD is extremely potent and can eliminate even the highest Toll signaling levels in the embryo, at the ventralmost region. When the domain of maximal Toll signaling was artificially enlarged by removing Serpin27A, which normally attenuates the activity of the Ea protease (Ligoxygakis et al., 2003), ectopic WntD was still able to abolish all signaling, indicating that it can overcome even elevated activation levels of the normal Toll pathway (Figures 2A and 2B). To determine the position of intersection by genetic epistasis, we combined ectopic (inhibitory) WntD with constitutive gain-of-function mutations in the Toll pathway.

A constitutively active form of the ligand Spz can be generated by expressing a secreted truncated version that is devoid of the N-terminal pro-domain (C-Spz) (Cho et al., 2010). Under these conditions, the dorsal part of the embryo that normally expresses *dpp* displays instead lateral genes such as *ind* (Haskel-Ittah et al., 2012). As a consequence, denticle bands, a cuticular structure indicative of a lateral cell fate, surround the entire embryonic circumference (Figures 2C and 2D). Co-expression of *C-spz* with *wntD* produced the typical dorsalized WntD overexpression outcome, leading to the formation of a smooth cuticle lacking denticles (Figures 2E and 2F). WntD is thus epistatic to C-Spz, implying that it blocks Toll signaling by directly attenuating the function of C-Spz, or of elements that act further downstream in the Toll pathway.

We next examined the consequences of expressing ectopic *wntD* together with activated versions of Toll. Signaling by Toll receptors involves formation of receptor dimers, which must adopt a productive conformation that can recruit downstream cytoplasmic adaptors. Binding of the Spz ligand favors the active dimer conformation, as does removal of the Toll extracellular domain, generating the constitutively active variant, $Toll^{\Delta LRR}$ (Gay et al., 2006; Winans and Hashimoto, 1995). Uniform $Toll^{\Delta LRR}$ expression gave rise to ventralized embryos, displaying maximal levels of nuclear Dl throughout their entire circumference. Correspondingly, these embryos did not form a cuticle, due to conversion of all cells to a mesodermal fate (Figures 2G and 2H). Importantly, this phenotype is maintained upon co-expression of *wntD* (Figures 2I and 2J), demonstrating that inhibition of signaling by ectopic WntD cannot be achieved in the absence of the extracellular domain of Toll. WntD is therefore likely to function extracellularly, by blocking either the Spz ligand or the Toll extracellular domain.

To distinguish between these scenarios, we used the dominant $Toll^{10b}$ allele, encoding a second constitutively acting variant of Toll. This mutant harbors a single missense mutation within an otherwise intact extracellular domain, which results in constitutive "activating dimerization," even in the absence of ligand (Schneider et al., 1991). In contrast to its inability to attenuate constitutive signaling by the $Toll^{\Delta LRR}$ variant, ectopic WntD significantly reduced the ventralizing effect of $Toll^{10b}$, so that the levels of Dl nuclear localization throughout the circumference of the embryo were only 50% of those observed following expression of $Toll^{\Delta LRR}$, compatible with partial formation of lateral cuticle (Figures 2K–2N). The capacity of WntD to attenuate signaling by $Toll^{10b}$ rules out the scenario of WntD acting via direct binding to Spz, since $Toll^{10b}$ acts in a ligand-independent manner. Rather, these observations imply that WntD, together with its receptor Fz4, affects Toll dimers directly by blocking their extracellular domain (Figures 2O and 2P).

The restriction of WntD inhibitory activity to the extracellular milieu is inconsistent with a distinct, and perhaps more intuitive scenario, in which binding of WntD to Fz4 elicits a signal transduction cascade that influences an intracellular step in Toll signaling. Accordingly, constitutive activation of canonical Wnt signaling by knockdown of *shaggy/ZW3* (Siegfried et al., 1992) had no effect on normal Toll signaling (Figure S2). Similarly, the lateralizing hyperactivation of Toll signaling that is achieved by eliminating Cactus, an intracellular inhibitor of Toll signaling that sequesters Dl in the cytoplasm (Isoda and Nusslein-Volhard, 1994; Roth et al., 1991), was epistatic to WntD overexpression (Figure S2).

Reduced Toll Variability Depends on Early, Posteriorly Localized *wntD* Expression

Since *sna* is induced at the beginning of nuclear cycle 14, we wanted to determine the expression pattern of *wntD* prior to this step, at a time when it can effectively influence the profile of *sna* expression. *wntD* RNA transcripts are detected in ~54% of early cycle-14 embryos, and are confined at this stage to a single patch at the posterior ventral side. This pattern can already be identified in younger embryos at cycles 12/13, and therefore represents the very first phase in the dynamic expression pattern of *wntD* reported earlier (Ganguly et al., 2005) (Figures 3A–3C).

Previous analysis of *wntD* expression has demonstrated that its compact enhancer architecture facilitates the convergence of two orthogonal signals (Helman et al., 2012; Figure 3D). A

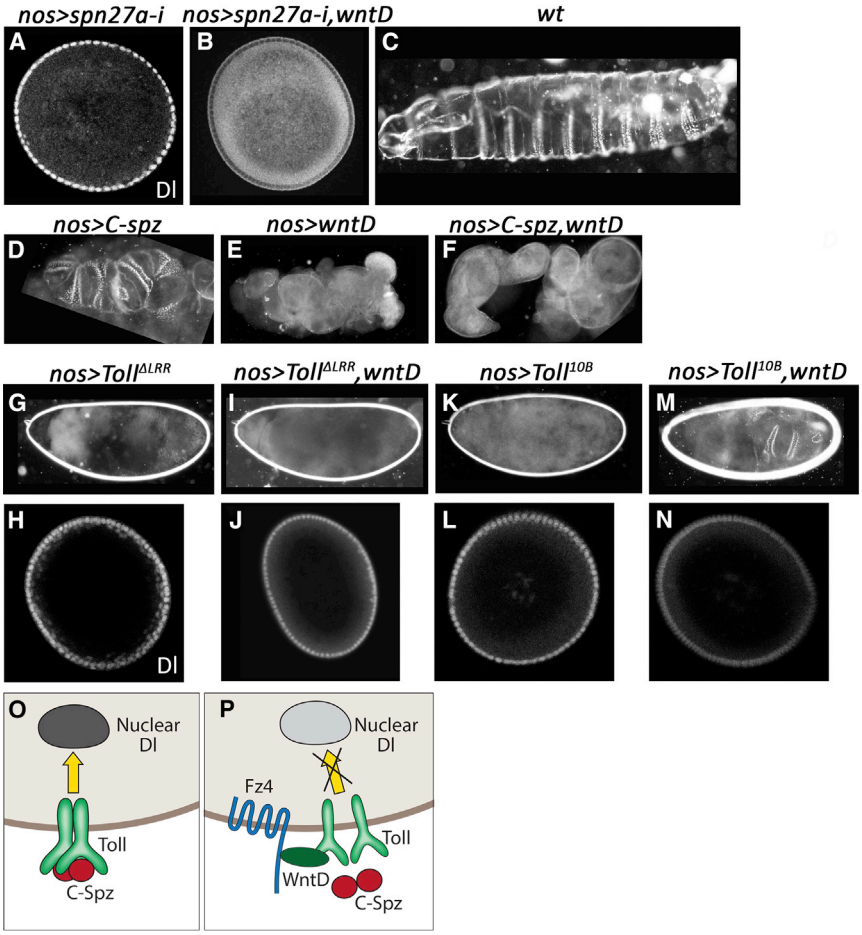

Figure 2. WntD/Fz4 Block the Toll Extracellular Domain

(A) Knockdown of *spn27a* in *nos-Gal4/UAS-spn27a RNAi* embryos leads to ubiquitous distribution of activated Ea, and uniformly high nuclear levels of Dl.

(B) Co-expression of *wntD* in this background was still able to overcome the increased activation of the Toll pathway and give rise to exclusion of Dl from all nuclei, highlighting the potency of ectopic WntD.

(C) Lateral (dark-field) view of the cuticle of a *wt* embryo. The lower, ventral aspect displays prominent bands of denticles, contrasting with the smooth appearance of the upper, dorsal surface.

(D) Cuticle of a *nos-Gal4/UAS-C-spz* embryo. Such ubiquitous expression of moderate levels of C-Spz leads to lateralization of the embryo, reflected by the formation of denticle bands around the entire embryo circumference.

(E) *nos-Gal4/UAS-wntD* embryos are dorsalized, as reflected by the absence of denticle bands.

(F) Upon co-expression of *C-spz* and *wntD*, the embryos remain dorsalized, indicating that WntD inhibits either C-Spz itself or elements downstream to it.

(G and H) Expression of constitutively active Toll lacking most of the extracellular domain, $Toll^{\Delta LRR}$, leads to uniform and high activation of the Toll pathway, resulting in strong ventralization of cell fates. This is reflected both by the absence of cuticle (G), and prominent nuclear localization of Dl (H) around the entire circumference, as all cells acquire a ventral-most, mesodermal fate.

(I and J) This ventralized phenotype was retained upon co-expression of *wntD*, indicating that WntD operates at the level of Toll or upstream to it.

(K and L) The dominant $Toll^{10b}$ allele leads to similar ventralization of the embryo.

(M and N) However, some attenuation of the ventralizing effect was achieved upon co-expression of *wntD*, as indicated by the appearance of cuticle and denticle bands, and a ~50% reduction in the uniform level of nuclear Dl. This effect indicates that WntD interacts with Toll to block the binding of C-Spz or receptor dimerization.

(O and P) Schematic representations of Toll signaling and the mechanism of WntD/Fz4 inhibition. (O) Binding of C-Spz to Toll triggers Dl nuclear localization. (P) WntD binds Fz4 and is presented to the extracellular domain of Toll, to block its association with C-Spz or dimerization, thus interfering with signaling into the embryo.

See also Figure S2.

binding site for Dl provides sensitivity to Toll signaling, whereas a binding site for Capicua (Cic) allows signaling only when this repressor is removed, following its phosphorylation by mitogen-activated protein kinase (MAPK). MAPK signaling first takes place at the embryonic termini, following activation of the Torso pathway (Gabay et al., 1997). Thus, signaling by Torso defines a highly restricted domain within the embryo, where the levels of Toll signaling can be sensed by the *wntD* enhancer. At the anterior end, substrate competition for MAPK phosphorylation between Cic and Bicoid leads to a delay in alleviating Cic repression (Kim et al., 2011). Thus, posterior expression of *wntD* precedes expression at the anterior. Finally, the *wntD* enhancer contains a consensus binding site for Zelda, a general facilitator of early zygotic gene expression (Foo et al., 2014). We assume that in the embryos that do not express *wntD* at early cycle 14, the levels of Toll signaling are below the required *wntD* threshold. This result is in accordance with the size distribution of the *sna* domain in *wntD* mutants (Figure 1E), where ~50% of the embryos retain values that are within the narrow range of *wt* embryos, and hence do not appear to require buffering.

Since *wntD* has a dynamic expression pattern (Ganguly et al., 2005), it was imperative to demonstrate that the earliest phase of its expression is the one responsible for modulating the variability in Toll signaling. Torso signaling is required only for the first phase of *wntD* expression, at the embryonic termini (Helman et al., 2012). We therefore monitored the variability of the *sna* domain in embryos laid by homozygous $torso^{1}$ or $torsolike^{4}$ (*tsl*) mutant females. The degree of *sna* variability in these mutants was similar to or even higher than that observed in w*ntD* mutants (Figures 3E and 3F). This indicates that the earliest expression of *wntD* at the termini is responsible for its capacity to attenuate the variability in Toll signaling. Notably, although Torso pathway mutants prevent *wntD* expression only at the termini of the embryo, the *sna* profile is altered throughout the entire anterior-posterior (AP) axis, as was observed following sectioning the embryos at their center. Therefore, local expression of *wntD* at the posterior

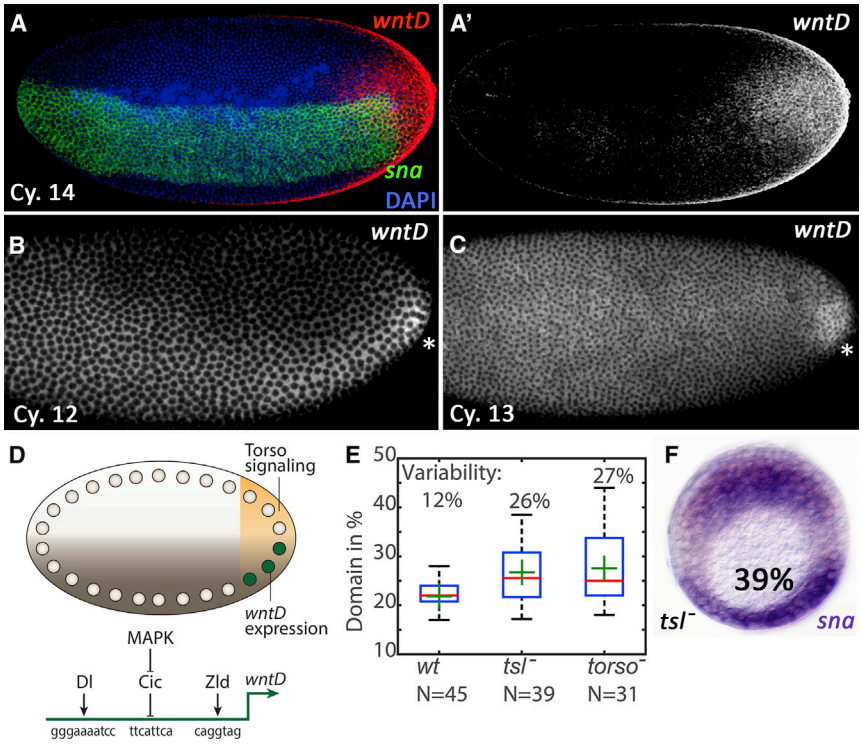

Figure 3. Early Posterior WntD Expression Buffers Toll Signaling

(A and A′) A ventrolateral view of an early cycle-14 embryo; anterior is to the left. *sna* expression (green) is observed ventrally, and expression of *wntD* is restricted to a posterior patch (red). Nuclei are visualized with DAPI (blue). This pattern represents the earliest zygotic expression domain of *wntD*, and is the one relevant for the attenuation of Toll signaling.

(B and C) Weak posterior expression of *wntD* can be detected in cycle-12 embryos, and is increased in cycle-13 embryos (asterisks).

(D) Scheme showing the posterior *wntD* expression domain at the intersection of the two orthogonal pathways, Toll that targets Dl to the nucleus, and Torso leading to MAPK phosphorylation and subsequent inactivation of the transcriptional repressor Cic. A consensus binding site for Zelda (Zld) facilitates early zygotic expression. Posterior *wntD* expression precedes the anterior expression due to substrate competition for MAPK by Bicoid.

(E and F) Since *wntD* expression requires activation of the Torso pathway, mutants in the Torso pathway give rise to variability in *sna* expression similar to the one observed in *wntD* mutants. In embryos derived from homozygous *torso*[1] or *torsolike*[4] (*tsl*) females, a significant variability in the size of the *sna* domain was observed, rising up to 45% of embryo circumference.

end normally impinges uniformly on Toll signaling throughout the entire embryo, consistent with rapid diffusion and equilibration of proteins (including secreted WntD) within the peri-vitelline fluid (Stein et al., 1991).

Posterior *wntD* expression is triggered by the intersection of the orthogonal Toll and Torso signaling cascades. To precisely define the boundaries of this domain, we quantified the relative level of nuclear Dl in the posterior cells that express *wntD* at cycle 14 (Figures 4A–4A″). In the most posterior cells that receive maximal Torso signaling, *wntD* is expressed in nuclei that display ~25% of maximal Dl nuclear localization. This represents the threshold level of nuclear Dl necessary for *wntD* expression. In the anterior-most part of the *wntD* expression domain, the levels of nuclear Dl reach ~65% of maximal Dl nuclear localization due to the morphology of the embryo. This value represents the upper limit of *wntD* expression as defined by the border of the Torso signaling domain.

WntD Buffers Variability through an Induction-Contraction Integral Feedback Loop

We used mathematical modeling to examine whether and under what conditions feedback through WntD can buffer the variability of the Toll-activation gradient. To this end, we modeled the interaction of WntD with Toll and its effect on Toll-activation levels (Modeling Supplement Figures MS1–MS3). Our model describes how embryo-to-embryo differences are buffered by a WntD-based integral feedback we term InC (Figure 4B). It also addresses the sources of variability in Toll signaling that are unmasked in *wntD*$^{-}$ mutant embryos.

Toll signaling (the Inducer) triggers expression of *wntD* (the Contractor), but only in a domain of intermediate Toll signaling levels (Figures 4A and 4B). WntD, in turn, evenly spreads throughout the entire extracellular fluid to globally adjust Toll signaling length scale, thus ensuring robustness. WntD binds Toll directly, and in doing so blocks the capacity of Toll to bind ligand, dimerize, and induce signaling. Note that, for simplicity, we neglect WntD interaction with Fz4.

To better understand the essence of the InC buffering mechanism, we first consider a one-dimensional approximation and then discuss the InC model implementation in the embryo. For the one-dimensional approximation we assume the following: the *wntD* expression zone is restricted to intermediate areas of Toll signaling, but WntD protein levels are nearly uniform throughout the extracellular milieu due to rapid diffusion, and globally affect the signaling gradient. We further assume WntD impacts on the morphogen gradient by modulating (contracting) its length scale and can thus approximate

$$M(x; \mathrm{WntD}, P) = M(x/\lambda(\mathrm{WntD}, P)), \qquad \text{(Equation 1)}$$

with M being the signaling level and λ the signaling profile length scale. λ depends on WntD as well as on all other, fluctuating parameters P in the system. Following the above considerations, steady state is achieved only when WntD stops accumulating and thus does not modulate λ further, which corresponds to

$$M(x^*/\lambda(\mathrm{WntD}^{st}, P)) = T^{\mathrm{WntD}}, \qquad \text{(Equation 2)}$$

with T^{WntD} denoting the threshold level allowing *wntD* expression, and x^* the relevant position where *wntD* expression is allowed (Figure 4C). Note that, in the context of the embryo, *wntD* is expressed only at the pole so that, in effect, at steady state $x^* > 0$ corresponding to intermediate Toll signaling levels. The main implication of Equation 2 is that at steady state, the

level of the Dl gradient at position x* is pinned to some fixed value that is independent of all other parameters. Since this pinning down of the gradient at one particular position is achieved by WntD-dependent modulation of the gradient length scale λ, it adjusts the profile globally to its desired pattern. The steady-state morphogen distribution is now buffered against variation in parameters. We term this mechanism ''Induction-Contraction'' or InC: the morphogen induces a widely diffusible molecule that functions to narrow down (or *contract*) the spread of the gradient. Clearly, this mechanism presents a general circuit topology that naturally buffers the morphogen gradient against fluctuations in morphogen length scale, which could be broadly applied to other morphogen-based systems.

The full model was formulated using a set of reaction-diffusion equations, and simulated on a curved two-dimensional surface of an ellipsoid using forward Euler, finite difference discretization (Figure 4D; see Modeling Supplement Figures MS2 and MS3). The requirement of Torso signaling for *wntD* expression was implemented by allowing *wntD* expression only in a restricted posterior domain (Figures 4D and 4E; Modeling Supplement Figures MS2 and MS3). Figures 4D and 4E show a simulation result, depicting Toll signaling throughout the embryo. For the full two-dimensional model (see Modeling Supplement), the dynamics of the buffering mechanism are similar to the one-dimensional approximation: Steady state was reached when Toll activity at the posterior-most embryonic region was reduced below the *wntD* expression threshold (Figure 4D, arrows). In this manner, the accumulating WntD effectively pinned the Toll activity levels to the specific threshold value, at this particular location (corresponding to a mid-gradient value along the embryo DV axis: Figures 4D and 4E). Since this pinning of the gradient was achieved by globally modulating the gradient length scale (via extracellular, spatially uniform WntD accumulation), the gradient adjusted to the desired profile throughout the embryo (Figures 4F–4H).

We simulated a population of 100 *wt* embryos with variable Toll signaling properties giving rise to variable shapes of the Toll signaling gradient. In this population, *wntD* expression was restricted to the pole, to recapitulate the normal noise-buffering capacity of InC. Comparison of the middle circumference Toll signaling profiles for these embryos and the distributions of *sna* domains with the corresponding *wntD*$^{-}$ mutant population shows a considerable reduction in variability and sharpening of the distribution in *wt* embryos (Figures 4I and 4J). Simulation results for the same population of embryos, only without the restriction on *wntD* expression at the pole, gave rise to Toll signaling profiles that peak at the *wntD* activation threshold (lower gray dotted line) and are below the *sna* activation threshold, giving rise to global shutdown of Toll signaling (Figure 4K). Parameter values used for this simulated population appear in Table S1.

To determine which properties significantly affect the profile of Toll signaling and might cause variability, we incorporated the mechanism of Spz gradient formation into our full model. In a recent study we described a model for the canonical DV patterning circuit, indicating that the Toll-activation gradient is established by self-organized shuttling (SOSH). SOSH described how an initially broad ventral signaling domain is refined by ligand shuttling, to generate a significantly narrower and sharper Toll-activation gradient (Haskel-Ittah et al., 2012). In the current study we address the robustness of the Toll-activation gradient formed by SOSH. We show that while being robust to most biological parameters (Figure S3), the Toll-activation gradient is still sensitive to variations in some parameters, most notably parameters associated with Spz and Toll expression and function, and the size of initial ventral pipe domain that defines the region of Spz processing (Figure S4). We utilize these findings to computationally establish the robustness InC introduces by challenging InC with variability in these parameters (see Modeling Supplement). Of the parameters to which SOSH is sensitive, η0 and Ttot represent protein levels for ligand and receptor, respectively, and are therefore most likely to be noisy in a population of embryos (Figure S3 and Modeling Supplement Table MS1). We therefore mostly focused on these two parameters when testing InC as a variability buffering mechanism. Our 2D surface numerical analysis of the model confirms that WntD-dependent feedback buffers the Toll-activation gradient against fluctuations in all model parameters (Figures 4D–4J and S4–S6).

The AP Signaling Gradient Depends on Embryo Morphology

The accuracy of variability buffering by InC depends on *wntD* expression being restricted to the same lower signaling level area in each embryo. This occurs when the decline in Toll signaling along the AP axis from middle to terminus is similar throughout the population (for this analysis we neglect Torso variability, which was measured to be low [Figure 5I]). To show this is indeed the case despite Toll variability between embryos, we compared the signaling decline along the AP axis in the simulated population. The similarity of the AP gradients in both *wt* and *wntD*$^{-}$ populations indicates that variability in signaling levels and *wntD* induction do not significantly affect the AP gradient (Figure S6). We can therefore conclude that the AP decline of Toll signaling is largely shaped by embryo morphology that is similar in the population, allowing InC to effectively buffer variability.

Variable Toll Signaling Induces a Corresponding Level of *wntD* mRNA

According to the InC model, *wntD* expression reduces variability by accumulating extracellular WntD protein until the Dl gradient attains its desired level. Thus, we expect early *wntD* expression to be highly variable among embryos, reflecting the initial (unbuffered) irregularities in Toll signaling. Conversely, *wntD* expression levels should be reduced later to an approximately uniform expression in the population, reflecting only the residual expression remaining once the desired steady-state profile of Toll signaling is achieved. We examined the variability in *wntD* expression by staining embryos for *wntD* RNA. Cycle 14 embryos can be staged with high temporal resolution according to the shape of their nuclei (Lecuit et al., 2002). We focused on embryos staged to the first 15 min of cycle 14, identified by the shape of their DAPI-stained nuclei in transverse sections taken at their center (Figures 5A–5C). Sections encompassing the posterior ends of the same embryos were isolated, and the number of nuclei expressing *wntD* (displaying masked DAPI levels) was quantified (Figures 5D and 5D′).

As expected, we find a large initial variability in the size of the posterior expression domain among embryos expressing *wntD*,

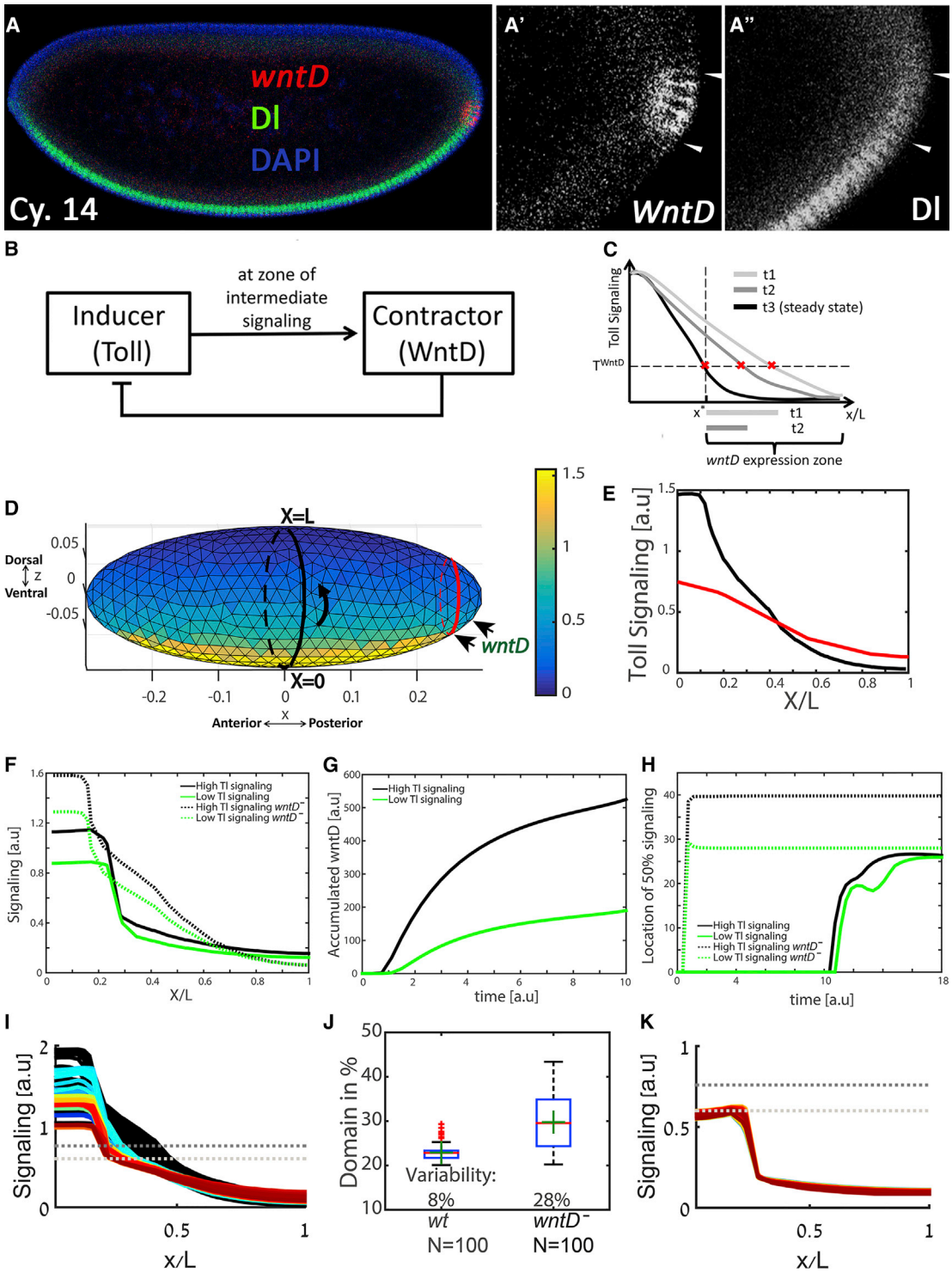

Figure 4. Restriction of Posterior WntD Expression Generates an Integral Feedback Loop

(A–A″) A lateral view of a cycle 14 embryo (anterior to the left) stained for *wntD* RNA (red), Dl (green), and nuclei (DAPI, blue) shows that *wntD* expression is confined to the posterior pole. (A′ and A″) Higher magnification views show that within the domain of *wntD* expression in this embryo (A′), nuclear levels of Dl (A″) range from ~65% of the maximal (ventral-most) levels to ~25% near the posterior pole (arrowheads), reflecting the border of the Torso signaling domain and the threshold of nuclear Dl for *wntD* expression, respectively.

(B) Scheme of induction-contraction integral feedback loop.

(C) Temporal dynamics of the Toll-activation gradient as it is shaped by InC in the one-dimensional approximation. At t1, *wntD* expression is induced by the global Toll signaling gradient only in the restricted *wntD* expression zone which is defined by x/L > x*/L and indicated. The size of *wntD* expression domain at t1 is also

(legend continued on next page)

ranging from 30 to 80 nuclei (Figures 5D, 5E, and 5J). The intensity of *wntD* expression within these cells appeared similar, indicating that alteration in WntD levels is achieved primarily by modulating the number of nuclei that will express this gene.

We wanted to examine whether the initial levels of Toll signaling determine the domain size of *wntD* expression, in a background where WntD would not impinge on its own expression. The experiment was carried out in *fz4* mutant embryos, where WntD cannot affect Toll signaling. Cycle 14 embryos were double stained for *wntD* RNA and Twi protein, and each embryo was dissected at the posterior end to determine the magnitude of *wntD* expression zone, and at the center to monitor the size of the Twi domain. We find a strong correlation between the level of Toll signaling and the size of the *wntD* domain, implying a causal relationship (Figures 5F–5H).

Because early *wntD* expression integrates orthogonal inputs from the Torso and Toll pathways, we wanted to test whether the measured variations are indeed associated primarily with differential initial Toll activation, as suggested by their tight correlation (Figure 5H). To monitor variability resulting specifically from Torso signaling, we measured *wntD* expression in embryos where Toll signaling is high and uniform throughout the entire embryo, following expression of the $Toll^{\Delta LRR}$ construct. In these embryos, *wntD* is expressed at the termini throughout the anterior and posterior caps (Figure 5I). When the size of the posterior domain (reflecting the level of Torso signaling) was determined, by counting the nuclei in the longest horizontal row expressing *wntD* (Figure 5I′), it showed a low level of variability between embryos, indicating that the Torso pathway is not a major contributor to variability in *wntD* expression (Figure 5K). Furthermore, incorporating this level of variability in Torso signaling into our simulations leads to only minor effects on *wntD* expression (Figures 5L and S6). We therefore conclude that the observed variability in *wntD* expression primarily reflects differences in Toll signaling, consistent with its predicted function as the buffering molecule of this cascade.

Variability in *wntD* Expression Is Reduced over Time

A key prediction of our model is that variability in *wntD* expression will be reduced in time. The levels of *wntD* at the onset of its expression correspond to the initial variable Toll signaling. However, the subsequent expression domain of *wntD* depends on and responds to the eventual, robust gradient. We therefore monitored the number of nuclei expressing *wntD* in *wt* and *fz4* mutant embryos, which were carefully timed during the first half of cycle 14. In the first 10–15 min, *wt* embryos showed a high variability, ranging from 30 to 80 nuclei. This variability was then dramatically reduced to 30–50 nuclei. In contrast, *fz4* mutant embryos, which are oblivious to WntD, displayed the same high level of variability throughout this period (Figures 6A and 6B). These results suggest that the feedback response of *wntD* expression is evident during the beginning of cycle 14.

Gene dosage alterations of *wntD* are expected to affect the production rate of the WntD protein. However, if the feedback response to *wntD* expression is effective by early cycle 14, as we predict, changes in *wntD* gene dosage would not alter the final outcome of *sna* expression domain. *wntD* gene dosage should only affect the length of time that the feedback requires to reach steady state, speeding up the buffering process for three copies and slowing it down for one copy. This is indeed seen in our numerical simulations (Figures 6C and 6D). We monitored experimentally the *sna* expression domain in embryo populations carrying one or three genomic copies of *wntD*. We find that the *sna* domain remains highly similar to that of *wt* embryos, when comparing both the mean expression domain and its variability between embryos (Figure 6E) as predicted by our model.

DISCUSSION

The early *Drosophila* embryo is surrounded by the peri-vitelline fluid, which provides a highly diffusible extracellular environment and thus constitutes a unique setting for execution of patterning. It is challenging to spatially restrict active extracellular components such as the protease Easter and processed ligand Spätzle in this environment (Ligoxygakis et al., 2003; Haskel-Ittah et al., 2012). On the other hand, rapid diffusion may facilitate global dispersion of other locally produced extracellular signals. This work demonstrates how the secreted WntD protein provides a buffering system for Toll signaling. Local induction of *wntD*

determined by Toll signaling levels, which must be above the threshold T^{WntD}. The expression zone according to these two conditions is indicated by the light-gray line below the plot. WntD protein diffuses rapidly and spreads uniformly throughout the one-dimensional tissue, globally contracting the Toll signaling gradient and giving rise to the narrower signaling profile at t2. WntD accumulation stops at t3 and steady state is reached, when the Toll gradient is sufficiently narrowed, such that the signaling levels in the relevant zone are below the T^{WntD} threshold.

(D) Numerical solution for Toll-activation levels on the curved surface of a three-dimensional ellipsoid representing the embryo. Signaling levels are indicated by the color bar. The posterior restriction of *wntD* expression confines it to lower levels of the Toll-activation gradient (arrows).

(E) Black: Toll-activation levels at the midline of the AP axis (corresponding to black circle in D). Red: Toll-activation levels at the edge of the *wntD* expression zone (red circle in D). Both plots are on a relative length axis: position divided by the length of the respective half circumference.

(F) Simulation of different initial levels of Toll signaling, and the resulting activation gradient in the presence or absence of WntD. The ventral-most point is denoted as 0. Note that presence of WntD makes the activation gradient of Toll sharper, and effectively buffers variability across most of the field.

(G) Simulation of the kinetics of WntD accumulation in the peri-vitelline fluid following high or low initial Toll signaling.

(H) Kinetics of Toll signaling defining the borders of *sna* expression, following high or low initial Toll signaling.

(I) Middle circumference Toll signaling profiles for 100 simulated embryos with variable randomized initial Toll signaling properties. *wt* embryos are colored, $wntD^{-}$ embryos are black (each mutant embryo has the same parameters as a corresponding *wt* embryo). The *wt* embryos have more similar signaling profiles around half-maximal signaling value than the $wntD^{-}$ embryos. This property corresponds to lower variability in the size of the *sna* domain. The two horizontal gray dotted lines represent the *sna* induction threshold (upper line) and *wntD* induction threshold (lower line). The values for these thresholds correspond to the measured *wntD* expression in (A).

(J) Variability of the relative size of *sna* expression domains in 100 simulated *wt* and $wntD^{-}$ embryos with variable randomized initial Toll signaling properties.

(K) Middle circumference Toll signaling profiles for the 100 simulated embryos from (I) without restriction of *wntD* production to the pole.

See also Modeling Supplement, Figures S3–S6.

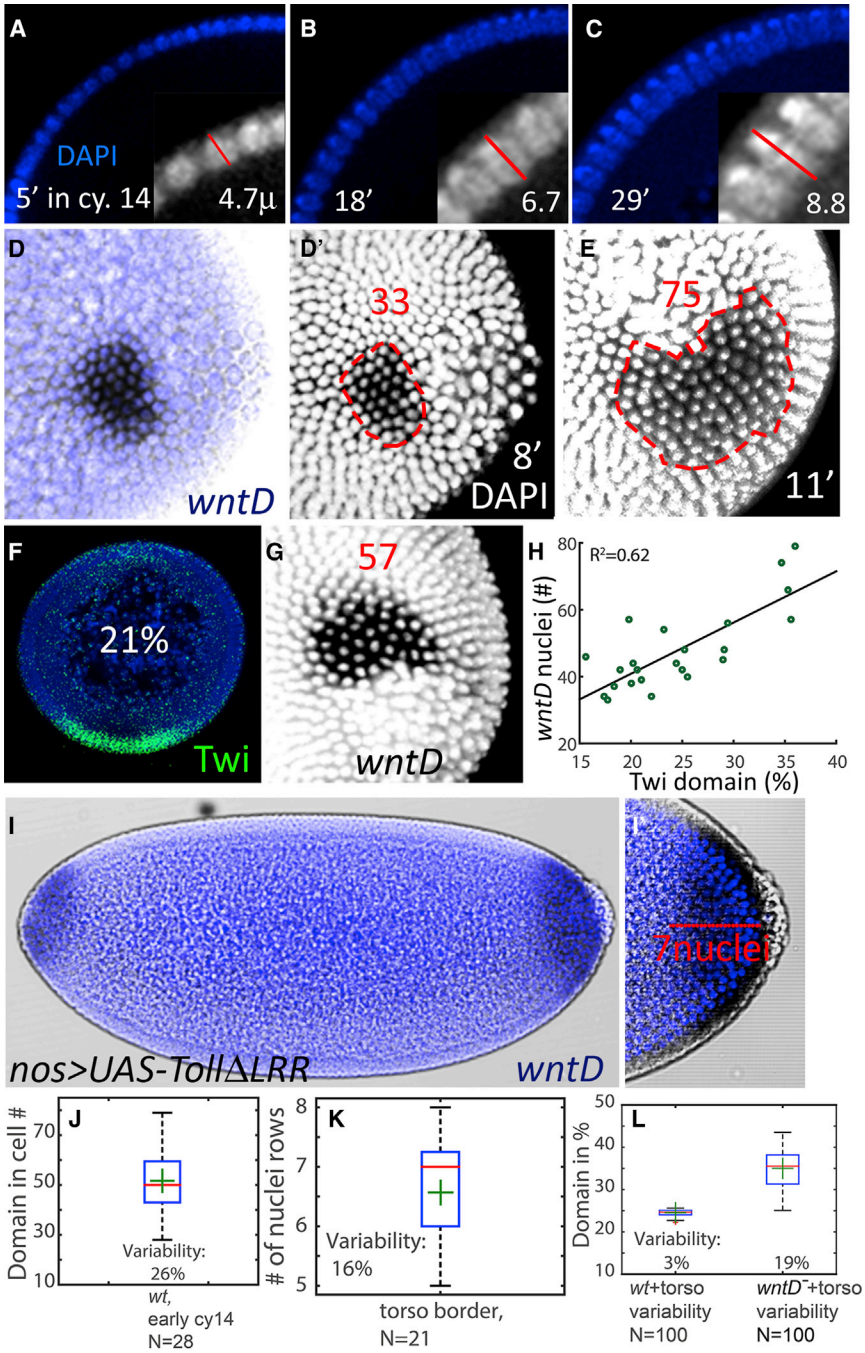

Figure 5. Variable Toll Signaling Induces a Corresponding Level of *wntD* mRNA

(A–C) The shape and height of DAPI-stained nuclei in a cross section provides an estimate for embryo age at cycle 14, with a resolution of minutes.

(D) The posterior cap of a DAPI-stained embryo, also monitored by in situ hybridization for *wntD* mRNA using alkaline phosphatase-based visualization.

(D′) The DAPI signal is partially masked by the *wntD* mRNA visualization method, allowing for precise quantification of nuclei within the *wntD* expression domain.

(D and E) A large variability between embryos in the number of nuclei expressing *wntD* is observed. (D) and (E) are 8 and 11 min into cycle 14, respectively.

(F and G) Cycle 14 *fz4* mutant embryos were stained for Twi protein, *wntD* RNA, and DAPI. Midsections and posterior caps from the same embryo revealed the size of the Twi domain and the number of nuclei expressing *wntD*, respectively.

(H) Plot of the correlation between the Twi domain size and the number of nuclei expressing *wntD* in individual embryos indicates that the initial level of Toll signaling determines the extent of *wntD* expression.

(I and I′) *wntD* expression was monitored in *nos-Gal4/UAS-Toll*$^{\Delta LRR}$ embryos, where Toll signaling was uniform and constitutive. The domain of expression that is induced by endogenous Torso signaling was assessed by counting the nuclei in the longest horizontal row expressing *wntD*, extending from the center of the pole cells.

(J) Variability in the number of nuclei expressing *wntD* in a population of *wt* embryos at early cycle 14.

(K) Toll signaling was activated uniformly and constitutively. For most embryos six to seven posterior nuclear rows expressed *wntD*, displaying a variability that is significantly lower than the one observed for expression of *wntD* in *wt* embryos. Hence, the major contribution to the variable levels of *wntD* can be attributed to the Toll pathway.

(L) Simulation of the distribution of *sna* borders, taking into account also the variability observed for Torso signaling, shows that a low variability in the *sna* domain can still be achieved. It is dramatically increased, however, in the absence of WntD.

See also Figure S6.

expression senses the initial level of Toll signaling, and attenuates Toll signaling globally by virtue of rapid diffusion and equilibration.

Buffering Variability: The Role of Posteriorly Restricted *wntD* Expression

The early patterning of the *Drosophila* embryo occurs along two axes, AP and DV, which remain largely independent. One clear manifestation of independent axial programs is that the DV gradient of Toll activation operates properly in mutants for the primary AP morphogen *bicoid* or its target gap genes. It was therefore quite surprising to identify the posteriorly localized aspect of *wntD* expression as the key for buffering variability in the Toll-activation gradient. Despite this restricted expression, buffering capacity is not confined to the posterior part of the embryo, but rather extends throughout the embryo. Indeed, removing either WntD or the Torso pathway, required for posterior *wntD* expression, significantly increased embryo-to-embryo variability in the profile of the Toll-activation gradient along the entire AP axis. No additional functions were attributed to this early *wntD* expression. What, then, could be the advantage of restricting *wntD* expression to the posterior pole?

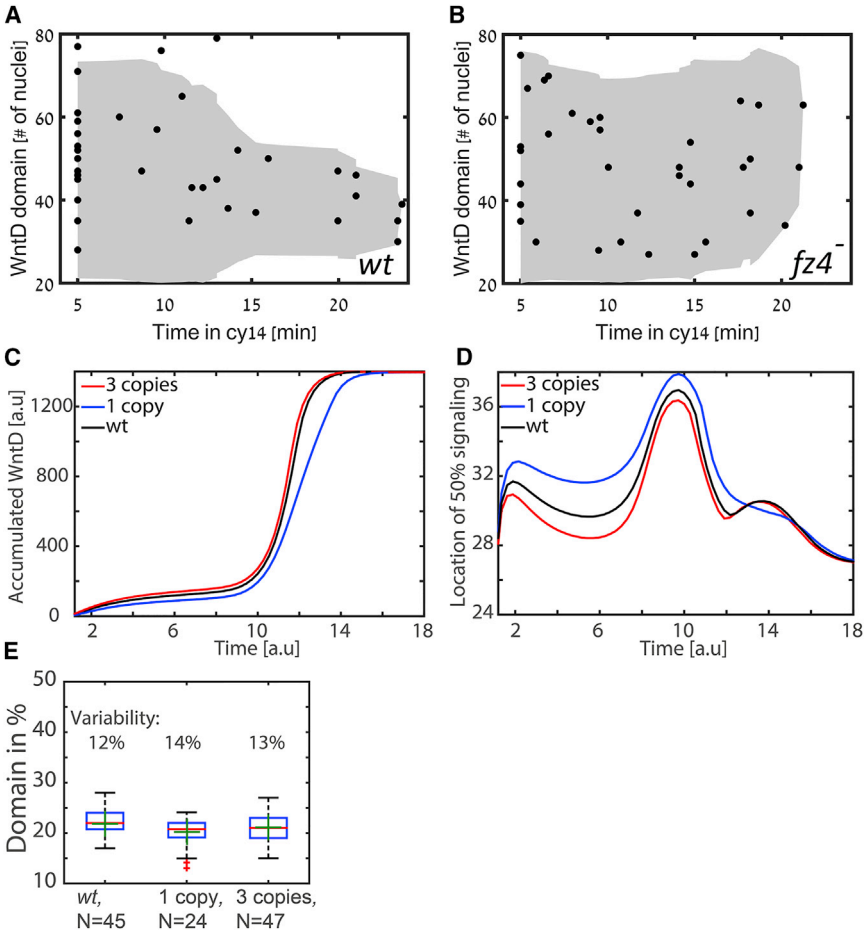

Figure 6. WntD Attenuates Its Own Expression

(A and B) Monitoring the number of nuclei expressing *wntD* in embryos progressing through cycle 14. Variability in the size of the *wntD* expression domain is markedly reduced by ~15 min in *wt* embryos (A), but persists in $fz4^{25\text{-}1}$ mutant embryos (B). Black dots are experimental measurements of individual embryos. Gray area denotes the calculated variability of measurements over time. Upper boundary is mean + 2SD, and lower boundary is mean − 2SD. For each time point the calculation was based on measurements at all subsequent times. The contraction of the gray area in (A) after 13 min indicates a decrease in the variability of the *wntD* expression domain.

(C) Implementation of an integral feedback at the relevant time frame raises the question of whether the system would be able to buffer variations in genomic *wntD* copy number. Simulations of accumulation of WntD in embryos carrying one to three copies show that, while the kinetics are different, the three genotypes converge to the same final level.

(D) Kinetics of the position of the 50% value of the Toll gradient shows fluctuations until the eventual convergence to the same position. Note that while the convergence was always obtained for a wide range of parameters tested, the actual dynamic profile in reaching this point varied. See Supplemental Information for details.

(E) The distribution of the size of the *sna* domain between embryos with 1, 2, or 3 genomic *wntD* copies was monitored and shows a similar profile for the three genotypes, consistent with the ability of the system to implement the feedback loop before the onset of *sna* expression. Note: Since flies with four genomic copies of *wntD* were sterile, the population of embryos with three copies was generated by crossing *wt* flies to flies with three *wntD* copies. Hence, only half of the embryo population carries three copies, but it does not show a deviation in *sna* expression compared with the parallel *wt* sample, where all embryos carry only two copies.

Our analysis suggests that posterior restriction of *wntD* expression is essential for the mechanism by which WntD buffers variability, adjusting the entire Toll-activation profile to its desired distribution (Figures 4I and 7). This buffering mechanism has three main attributes. First, WntD is stable and rapidly diffusible. Second, WntD functions globally to contract and reduce the spread of the Toll-activation profile. Finally, induction of WntD expression is confined to intermediate but not maximal levels of Toll signaling. Buffering adjusts the Toll-activation gradient as follows: a wide initial Toll gradient allows WntD accumulation, leading to global contraction of the gradient and thereby narrowing down the region in which *wntD* can be expressed, until a fixed steady-state profile is reached. We term this circuit InC.

Notably, the ability of the InC circuit to buffer variability by properly adjusting the gradient relies on restricting the contractor expression domain to a region that is not exposed to the maximal levels of Toll activation. Such confined expression is required to ensure that expression of the contractor molecule will be fully inhibited when morphogen levels at a defined position $x^* > 0$ within the field decrease below the contractor expression threshold. In this manner, the Toll-activation level at position x^* is set to some desired level. Since this pinning is achieved by modulating the morphogen gradient length scale (by accumulation of the contractor), it will ensure adjustment of the entire profile. Clearly, such pinning will lose its effectiveness if employed at the maximal level of the gradient $x^* = 0$, which is less dependent on the gradient length scale, and will lead to a global shutdown of Toll signaling.

In the case of *wntD*, expression is prevented from the regions of highest Toll activation by enabling only posterior expression. Indeed, as observed experimentally and verified by our three-dimensional simulation, the geometry of the embryo ensures that the highest levels of Toll activation within the posterior pole correspond to intermediate levels (compared with the maximal levels found in the ventral-most part in mid-embryo sections). Therefore, the geometry of the embryo plays an important role in implementing the InC buffering circuit.

Buffering Variability using Integral Feedback: The InC versus Expansion-Repression Circuits

The InC mechanism is conceptually analogous to the Expansion-Repression (ExR) circuit we recently described for scaling a morphogen gradient with tissue size, and which likely functions for scaling the Dpp morphogen gradient in the wing imaginal disc (Ben-Zvi and Barkai, 2010; Ben-Zvi et al., 2011). In both cases, the feedback molecule (contractor or expander) is stable,

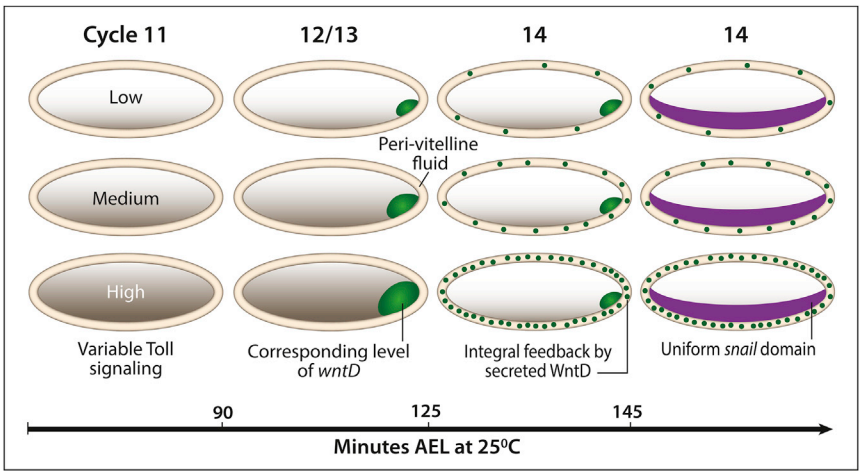

Figure 7. A WntD-Dependent Integral Feedback Loop Attenuates Variability in Toll Signaling

Embryos initially display a large variability in maternally based Toll signaling (gray). At nuclear cycles 12/13, the initial level of Toll signaling dictates the number of nuclei that will zygotically express *wntD* (green) at the posterior pole of the embryo. Expression of *wntD* is confined to the posterior pole at this stage, since it also requires the activation of the terminal Torso pathway that removes the Cic repressor. Although expression is spatially restricted, the WntD protein is readily secreted to the peri-vitelline fluid, where it rapidly diffuses and equilibrates. Binding of WntD/Fz4 to the Toll receptor competes with the binding of C-Spz and dimerization, thus attenuating Toll pathway signaling. The level of WntD will increase until Toll signaling reaches a fixed profile where WntD shuts off its own expression, generating an integral feedback loop. Induction of *wntD* is restricted to intermediate levels of Toll signaling by the parallel requirement for Torso signaling. This generates a regulatory topology we term Induction-Contraction, which facilitates a robust and invariable Toll signaling profile within the population of embryos, as reflected by the fixed relative size of the *sna* and *twi* expression domains (purple). AEL, after egg laying.

diffuses rapidly, and accumulates until the morphogen profile reaches some threshold. Both globally affect the morphogen spread by modulating the gradient length scale. ExR achieves scaling by effectively implementing an integral feedback loop (Ben-Zvi and Barkai, 2010; Ben-Zvi et al., 2011; Hamaratoglu et al., 2011). This holds true also for the InC circuit: contractor accumulation depends on the difference between actual and desired morphogen gradient length scale (the "error"), and its value (the integrated error) triggers the feedback to correct this length scale, until the desired steady-state profile is reached.

ExR and InC have opposite effects on the signaling gradient: ExR expands the gradient, and is therefore applicable to cases where the initial, unbuffered gradient is narrow. In contrast, InC constricts the gradient and is thus relevant to cases where the initial gradient is broad. This makes the InC better suited for buffering variations in the DV gradient, since this early gradient begins in a wide domain where the Ea protease is activated (Cho et al., 2012), and must be formed and adjusted to a significantly narrower domain. This refinement is achieved by restricting diffusion of activated Ea (Ligoxygakis et al., 2003), and by a self-organized ligand shuttling mechanism (Haskel-Ittah et al., 2012), but could be further assisted by the InC feedback. In contrast, in more typically described cases, the morphogen spreads from a restricted source, and its distribution should be broadened rather than constrained, calling for the use of the ExR module.

An additional difference between the two modules concerns the mechanism defining the expression domain of the feedback molecule. The expander in ExR is naturally expressed only at the edge of the field, where it is not repressed by the morphogen. Conversely, in the InC circuit, induction needs to be confined to a region exposed to lower morphogen levels, thus requiring an additional, morphogen-independent trigger, such as Torso signaling in the case of *wntD*. In this sense, ExR is more general and easier to implement than InC.

The WntD Buffering Mechanism

A critical requirement for the InC mechanism is the rapid diffusion of the contractor (WntD), leading to its approximately uniform concentration throughout the embryo. Several features contribute to the capacity of locally produced WntD to affect Toll signaling in the entire embryo. The *wntD* gene is compact with no introns and a short regulatory sequence, allowing for rapid transcription. The WntD protein does not undergo the post-translational modifications common to other Wnt proteins, and is hence readily trafficked within the embryo and secreted (Ching et al., 2008). The environment of the peri-vitelline fluid is highly diffusible, as was shown by equilibration of labeled BSA within 5–10 min (Stein et al., 1991). Finally, WntD exerts its influence directly within the extracellular milieu following binding to Fz4 and Toll, without the need to trigger an intracellular signaling pathway. Thus, despite the limited time of less than an hour between the onset of *wntD* expression and the induction of *sna*, the attenuating WntD signal equilibrates around the embryo within the peri-vitelline fluid.

An additional requirement is that the contractor will function by modulating the gradient length scale. In the case of WntD, our epistasis experiments map the interaction between the WntD and Toll pathways to the Toll receptor itself. WntD therefore inhibits Toll activation. Importantly, inhibition at the level of the Toll receptor not only attenuates signaling but also provides an additional feature by specifically affecting the gradient length scale. Our simulations assume that WntD inhibits Toll activity by blocking its extracellular domain. This not only reduces downstream activation, but also facilitates a steeper distribution of Spz. When active Spz is shuttled, its release depends on the local balance between the inhibitory Spz pro-domain (N-Spz) and accessible Toll. Partial blocking of Toll receptors by WntD will contribute to further restrict release of Spz for productive Toll binding within the ventral-most region. WntD therefore decreases the gradient length scale in a concentration-dependent manner, as required by the InC circuit, and makes the Toll-activation gradient sharper. In this capacity, it further refines the gradient of C-Spz distribution that is generated by SOSH (Haskel-Ittah et al., 2012).

Sources of Variability

The extent of variability in developmental patterning may differ for distinct signaling pathways or biological scenarios. For

example, when we monitored the expression of *wntD* under conditions where Toll activation was constitutive, the size of the expression domain at the embryonic termini depended strictly on the level of Torso signaling, and showed only moderate variability between embryos (Figures 5I′ and 5K). Conversely, removal of two feedback elements participating in early embryonic BMP signaling uncovered a high level of inherent variability (Gavin-Smyth et al., 2013).

The large degree of variability that was exposed in the *wntD/fz4* mutant backgrounds was surprising. This variability was observed between embryos, but not within the same embryo, when comparing different positions along the AP axis. What could be the source of variability in Toll signaling? While variability in the levels of maternal transcripts encoding the components of the Toll pathway may be involved, we view this option as less likely. Quantitation of variability of the number of *bicoid* transcripts that are deposited into individual eggs has demonstrated a relatively low variability of only ~9% (Petkova et al., 2014). Since most maternal transcripts are present in the egg in about 1 million copies, random fluctuations in their levels are not likely to play a significant role. We are currently exploring the possibility that fluctuations in the size of the domain where *pipe* is expressed during oogenesis (Sen et al., 1998) provide a major source of variability (Figures S3 and S4). Other possibilities include size differences between embryos or between the developing oocytes. Importantly, the InC circuit we described buffers against all of these forms of variability, making the gradient essentially independent of many different stochastic, genetic, or environmental variations.

EXPERIMENTAL PROCEDURES

Probes and Antibodies

Probes and hybridization for *sna* or *twi* were carried out as in Haskel-Ittah et al. (2012). Fluorescent in situ hybridization was carried out with an RNA fluorescein isothiocyanate (FITC)-labeled probe that was synthesized with T7 enzyme. For fluorescent detection, an anti-FITC-horseradish peroxidase (HRP) conjugated antibody was used. The *wntD* expression domain was detected via a digoxigenin (DIG)-labeled DNA probe, followed by anti-DIG-alkaline phosphatase conjugated antibody and substrate detection (Roche), or fluorescent detection using anti-DIG-HRP or anti-DIG-alkaline phosphatase conjugated antibodies according to Shwartz and Zelzer (2014). Hybridization was carried out at 55°C for DNA probes or 60°C when an RNA probe was used. For simultaneous detection of RNA and protein, the embryos were treated according to Helman et al. (2012). Anti-Dl antibodies were used (mouse 1:25, Developmental Studies Hybridoma Bank), followed by anti-mouse Alexa 488 secondary antibodies (1:800, Molecular Probes). Rat anti-Twi antibody (obtained from E. Wieschaus) was diluted 1:500, followed by anti-rat Alexa 488 secondary antibodies (1:800, Molecular Probes). Signal enhancer (Molecular Probes lot #1453392) was added to all fluorescent stainings.

Fly Strains

$wntD^{KO1}$ (Gordon et al., 2005), $fz4^{25\text{-}1}$ (McElwain et al., 2011), *nos-Gal4*, *UASp-wntD* (Gordon et al., 2005), *UASp-spn27a RNAi* (used at 29°C, obtained from P. Ligoxygakis), and *UASp-C-Spz-GFP* (Cho et al., 2010). $Toll^{\Delta LRR}$ (Winans and Hashimoto, 1995) was cloned by PCR, inserted into a UASp-attB plasmid, and integrated into the AttP40 site. Other strains were $Toll^{10b}$, *UAS-sgg* RNAi (TRIP GL002977), *UAS-Cact* RNAi (VDRC 34775), $torso^{1}$, and $torsolike^{4}$. To generate flies carrying three copies of *wntD*, we integrated attB-P[acman]-CmR-BW-09A09 carrying the complete *wntD* genomic region into the AttP2 site.

Modeling Approach

The governing reaction-diffusion equations for the model were numerically solved using a standard (forward Euler) finite difference scheme on the surface of an ellipsoid that represents the *Drosophila* embryo. This surface was meshed using a MATLAB implementation of the Delaunay triangulation routine, and the Laplace-Beltrami operator was calculated using the cotangent weights scheme, implemented in the MATLAB Toolbox Graph (Peyre, 2007).

Simulation Scenarios and Parameter Values for Main Text Figures

For Figures 4D–4H, full model equations were solved and temporal dynamics or steady state were plotted. The parameters used were based on Table S3. For High and low Toll signaling sets, 10% to η_0 and T_{tot} values were added/subtracted, respectively. For Figures 4I–4K, 100 *wt* embryos were simulated: for each embryo all parameters were set to Table S1 values and variability was added to η_0 and T_{tot} by randomly drawing η_0 and T_{tot} from a normal distribution with a mean of standard η_0 and T_{tot} values (Table S1) and an SD of 15% times the respective mean. This ratio between the SD and the mean was denoted in % as the variability percent. The respective 100 $wntD^{-}$ embryos were generated by setting $\beta_w = 0$. For each embryo middle circumference signaling was calculated (Modeling Supplement Figure MS3). In Figure 4K, restriction of WntD production to the pole was not implemented.

For Figure 5, 100 *wt* embryos were simulated, for each embryo all parameters were set to Table S3 values, and variability to η_0 and T_{tot} with a 15% variability percent was then added. Also, for each embryo the x location of the Torso border was chosen by randomly drawing from a uniform distribution with minimal and maximal values that correspond to the respective values measured in vivo (Figure 5H). The respective 100 $wntD^{-}$ embryos were then generated by setting $\beta_w = 0$.

For Figure 6 full model equations were solved, and temporal dynamics of WntD accumulation and the location of 50% signaling were plotted. The *wt* parameter set was based on Table S3. For three or one genomic copies of *wntD*, β_w was multiplied by 1.5 or 0.5, respectively.

SUPPLEMENTAL INFORMATION

Supplemental Information includes six figures, three tables, and a modeling supplement and can be found with this article online at http://dx.doi.org/10.1016/j.devcel.2016.01.023.

AUTHOR CONTRIBUTIONS

Conceptualization, N.R., I.A., M.H.-I., N.D., E.D.S., N.B., and B.-Z.S.; Investigation, N.R., M.H.-I., and N.D.; Methodology and Software, I.A.; Writing, I.A., N.B., and B.-Z.S.; Supervision and Funding Acquisition, E.D.S., N.B., and B.-Z.S.

ACKNOWLEDGMENTS

We are grateful to Roel Nusse for providing the *wntD* and *fz4* alleles and constructs, Petros Ligoxygakis for the *spn27a* RNAi line, and Eric Wieschaus for Twi antibody. We thank Ze'ev Paroush for stimulating and insightful discussions throughout this work, and members of the Shilo and Barkai labs for ideas and comments. We thank Shari Carmon for help and Orit Bechar for graphics. B.S. and E.S. were supported by grants from the Minerva Foundation, the Kahn Center for Systems Biology, and the Schoenheimer Foundation. N.B. was supported by a grant from the ERC. B.S. is an incumbent of the Hilda and Cecil Lewis chair for Molecular Genetics, N.B. is an incumbent of the Lorna Greenberg Scherzer Professorial Chair.

Received: July 13, 2015
Revised: November 22, 2015
Accepted: January 27, 2016
Published: February 22, 2016

REFERENCES

Barkai, N., and Shilo, B.Z. (2009). Robust generation and decoding of morphogen gradients. Cold Spring Harb. Perspect. Biol. *1*, a001990.

Ben-Zvi, D., and Barkai, N. (2010). Scaling of morphogen gradients by an expansion-repression integral feedback control. Proc. Natl. Acad. Sci. USA *107*, 6924–6929.

Ben-Zvi, D., Pyrowolakis, G., Barkai, N., and Shilo, B.Z. (2011). Expansion-repression mechanism for scaling the Dpp activation gradient in *Drosophila* wing imaginal discs. Curr. Biol. *21*, 1391–1396.

Ching, W., Hang, H.C., and Nusse, R. (2008). Lipid-independent secretion of a *Drosophila* Wnt protein. J. Biol. Chem. *283*, 17092–17098.

Cho, Y.S., Stevens, L.M., and Stein, D. (2010). Pipe-dependent ventral processing of Easter by Snake is the defining step in *Drosophila* embryo DV axis formation. Curr. Biol. *20*, 1133–1137.

Cho, Y.S., Stevens, L.M., Sieverman, K.J., Nguyen, J., and Stein, D. (2012). A ventrally localized protease in the *Drosophila* egg controls embryo dorsoventral polarity. Curr. Biol. *22*, 1013–1018.

Foo, S.M., Sun, Y., Lim, B., Ziukaite, R., O'Brien, K., Nien, C.Y., Kirov, N., Shvartsman, S.Y., and Rushlow, C.A. (2014). Zelda potentiates morphogen activity by increasing chromatin accessibility. Curr. Biol. *24*, 1341–1346.

Gabay, L., Seger, R., and Shilo, B.Z. (1997). MAP kinase in situ activation atlas during *Drosophila* embryogenesis. Development *124*, 3535–3541.

Ganguly, A., Jiang, J., and Ip, Y.T. (2005). *Drosophila* WntD is a target and an inhibitor of the Dorsal/Twist/Snail network in the gastrulating embryo. Development *132*, 3419–3429.

Gavin-Smyth, J., Wang, Y.C., Butler, I., and Ferguson, E.L. (2013). A genetic network conferring canalization to a bistable patterning system in *Drosophila*. Curr. Biol. *23*, 2296–2302.

Gay, N.J., Gangloff, M., and Weber, A.N. (2006). Toll-like receptors as molecular switches. Nat. Rev. Immunol. *6*, 693–698.

Gordon, M.D., Dionne, M.S., Schneider, D.S., and Nusse, R. (2005). WntD is a feedback inhibitor of Dorsal/NF-kappaB in *Drosophila* development and immunity. Nature *437*, 746–749.

Hamaratoglu, F., de Lachapelle, A.M., Pyrowolakis, G., Bergmann, S., and Affolter, M. (2011). Dpp signaling activity requires Pentagone to scale with tissue size in the growing *Drosophila* wing imaginal disc. PLoS Biol. *9*, e1001182.

Haskel-Ittah, M., Ben-Zvi, D., Branski-Arieli, M., Schejter, E.D., Shilo, B.Z., and Barkai, N. (2012). Self-organized shuttling: generating sharp dorsoventral polarity in the early *Drosophila* embryo. Cell *150*, 1016–1028.

Helman, A., Lim, B., Andreu, M.J., Kim, Y., Shestkin, T., Lu, H., Jimenez, G., Shvartsman, S.Y., and Paroush, Z. (2012). RTK signaling modulates the Dorsal gradient. Development *139*, 3032–3039.

Herr, P., and Basler, K. (2012). Porcupine-mediated lipidation is required for Wnt recognition by Wls. Dev. Biol. *361*, 392–402.

Isoda, K., and Nusslein-Volhard, C. (1994). Disulfide cross-linking in crude embryonic lysates reveals three complexes of the *Drosophila* morphogen dorsal and its inhibitor cactus. Proc. Natl. Acad. Sci. USA *91*, 5350–5354.

Kanodia, J.S., Rikhy, R., Kim, Y., Lund, V.K., DeLotto, R., Lippincott-Schwartz, J., and Shvartsman, S.Y. (2009). Dynamics of the Dorsal morphogen gradient. Proc. Natl. Acad. Sci. USA *106*, 21707–21712.

Kim, Y., Andreu, M.J., Lim, B., Chung, K., Terayama, M., Jimenez, G., Berg, C.A., Lu, H., and Shvartsman, S.Y. (2011). Gene regulation by MAPK substrate competition. Dev. Cell *20*, 880–887.

Lagha, M., Bothma, J.P., Esposito, E., Ng, S., Stefanik, L., Tsui, C., Johnston, J., Chen, K., Gilmour, D.S., Zeitlinger, J., et al. (2013). Paused Pol II coordinates tissue morphogenesis in the *Drosophila* embryo. Cell *153*, 976–987.

Lecuit, T., Samanta, R., and Wieschaus, E. (2002). Slam encodes a developmental regulator of polarized membrane growth during cleavage of the *Drosophila* embryo. Dev. Cell *2*, 425–436.

Liberman, L.M., Reeves, G.T., and Stathopoulos, A. (2009). Quantitative imaging of the Dorsal nuclear gradient reveals limitations to threshold-dependent patterning in *Drosophila*. Proc. Natl. Acad. Sci. USA *106*, 22317–22322.

Ligoxygakis, P., Roth, S., and Reichhart, J.M. (2003). A serpin regulates dorsal-ventral axis formation in the *Drosophila* embryo. Curr. Biol. *13*, 2097–2102.

McElwain, M.A., Ko, D.C., Gordon, M.D., Fyrst, H., Saba, J.D., and Nusse, R. (2011). A suppressor/enhancer screen in *Drosophila* reveals a role for wnt-mediated lipid metabolism in primordial germ cell migration. PLoS One *6*, e26993.

Moussian, B., and Roth, S. (2005). Dorsoventral axis formation in the *Drosophila* embryo—shaping and transducing a morphogen gradient. Curr. Biol. *15*, R887–R899.

Petkova, M.D., Little, S.C., Liu, F., and Gregor, T. (2014). Maternal origins of developmental reproducibility. Curr. Biol. *24*, 1283–1288.

Peyre, G. (2007). Toolbox Graph—Graph Theory Toolbox (Gabriel Peyre).

Rogers, K.W., and Schier, A.F. (2011). Morphogen gradients: from generation to interpretation. Annu. Rev. Cell Dev. Biol. *27*, 377–407.

Roth, S., Stein, D., and Nusslein-Volhard, C. (1989). A gradient of nuclear localization of the dorsal protein determines dorsoventral pattern in the *Drosophila* embryo. Cell *59*, 1189–1202.

Roth, S., Hiromi, Y., Godt, D., and Nusslein-Volhard, C. (1991). cactus, a maternal gene required for proper formation of the dorsoventral morphogen gradient in *Drosophila* embryos. Development *112*, 371–388.

Rushlow, C.A., Han, K., Manley, J.L., and Levine, M. (1989). The graded distribution of the dorsal morphogen is initiated by selective nuclear transport in *Drosophila*. Cell *59*, 1165–1177.

Schneider, D.S., Hudson, K.L., Lin, T.Y., and Anderson, K.V. (1991). Dominant and recessive mutations define functional domains of Toll, a transmembrane protein required for dorsal-ventral polarity in the *Drosophila* embryo. Genes Dev. *5*, 797–807.

Sen, J., Goltz, J.S., Stevens, L., and Stein, D. (1998). Spatially restricted expression of pipe in the *Drosophila* egg chamber defines embryonic dorsal-ventral polarity. Cell *95*, 471–481.

Shilo, B.Z., Haskel-Ittah, M., Ben-Zvi, D., Schejter, E.D., and Barkai, N. (2013). Creating gradients by morphogen shuttling. Trends Genet. *29*, 339–347.

Shwartz, Y., and Zelzer, E. (2014). Nonradioactive in situ hybridization on skeletal tissue sections. Methods Mol. Biol. *1130*, 203–215.

Siegfried, E., Chou, T.B., and Perrimon, N. (1992). Wingless signaling acts through zeste-white 3, the *Drosophila* homolog of glycogen synthase kinase-3, to regulate engrailed and establish cell fate. Cell *71*, 1167–1179.

Stein, D.S., and Stevens, L.M. (2014). Maternal control of the *Drosophila* dorsal-ventral body axis. Wiley Interdiscip. Rev. Dev. Biol. *3*, 301–330.

Stein, D., Roth, S., Vogelsang, E., and Nusslein-Volhard, C. (1991). The polarity of the dorsoventral axis in the *Drosophila* embryo is defined by an extracellular signal. Cell *65*, 725–735.

Steward, R. (1989). Relocalization of the dorsal protein from the cytoplasm to the nucleus correlates with its function. Cell *59*, 1179–1188.

Waddington, C.H. (1959). Canalization of development and genetic assimilation of acquired characters. Nature *183*, 1654–1655.

Willert, K., and Nusse, R. (2012). Wnt proteins. Cold Spring Harb. Perspect. Biol. *4*, a007864.

Winans, K.A., and Hashimoto, C. (1995). Ventralization of the *Drosophila* embryo by deletion of extracellular leucine-rich repeats in the Toll protein. Mol. Biol. Cell *6*, 587–596.